

Colloidal Lattice Shearing and Rupturing with a Driven Line of Particles

A. Libál^{1,2}, B.M. Csíki², C. J. Olson Reichhardt¹, and C. Reichhardt¹

¹*Theoretical Division, Los Alamos National Laboratory, Los Alamos, New Mexico 87545 USA*

²*Faculty of Mathematics and Computer Science,
Babes-Bolyai University, RO-400591 Cluj-Napoca, Romania*

(Dated: June 24, 2018)

We examine the dynamics of two-dimensional colloidal systems using numerical simulations of a system with a drive applied to a thin region in the middle of the sample to produce a local shear. For a monodisperse colloidal assembly, we find a well defined decoupling transition separating a regime of elastic motion from a plastic phase where the particles in the driven region break away or decouple from the particles in the bulk, producing a shear band. For a bidisperse assembly, we find that the onset of a bulk disordering transition coincides with the broadening of the shear band. We identify several distinct dynamical regimes that are correlated with features in the velocity-force curves. As a function of bidispersity, the decoupling force shows a nonmonotonic behavior associated with features in the noise fluctuations, power spectra, and bulk velocity profiles. When pinning is added in the bulk, we find that the shear band regions can become more localized, causing a decoupling of the driven particles from the bulk particles. For a system with thermal noise and no pinning, the shear band region becomes more extended and the average velocity of the driven particles drops at the thermal disordering transition of the bulk system.

PACS numbers: 82.70.Dd, 83.80.Hj

I. INTRODUCTION

As the ability to manipulate small particles or groups of small particles has advanced, there have been a growing number of studies examining the effect of local perturbations such as driving a single probe particle through a particle assembly in colloidal^{1–14} and granular^{15–19} media. The fluctuations and transport characteristics of the probe particle can undergo pronounced changes depending on the ordering of the surrounding media, the particle-particle interactions, the temperature, and the magnitude of the external force on the probe particle.

In systems with short range interactions such as disks or granular particles^{15–19}, the velocity of the probe particle can drop under even a small change in the bulk media density as the jamming transition is approached. For bulk densities below jamming, the external force needed to move the probe particle is small or absent and the probe particle velocity distribution is bimodal¹⁹. Close to jamming, the external force needed to push the probe particle through the medium becomes finite and rapidly increases, while the velocity fluctuations are intermittent and have a power law distribution that has been interpreted as arising due to criticality associated with the jamming transition^{2,15,16,18,19}.

For systems with longer range interactions such as charged colloids, there is an elastic or coupled flow regime at low drives where the probe particle drags the entire assembly of particles without any local tearing⁴³. At higher drives there can be a well defined transition to a plastic response regime where the probe particle induces tearing rearrangements in the surrounding media, and the velocity of the probe particle differs from that of the particles it is dragging. The velocity-force curves in these systems can be used to identify the critical driving force separat-

ing the elastic and plastic regimes. The velocity increases as a power law with increasing external force in the plastic regime, similar to the behavior observed for plastic depinning of vortices²⁰ and colloids⁴⁴ in the presence of quenched disorder.

It is also possible to consider the motion of a forced particle through a surrounding medium in the presence of quenched disorder. Such a situation has been studied for dragging individual vortices in type-II superconductors^{21–24}, where a driven vortex interacts with the intrinsic pinning in the sample as well as with the surrounding vortices. In this case, the probe particle can be indirectly pinned due to its interaction with bulk particles that are strongly directly pinned by the substrate, causing the appearance of a threshold depinning force for the probe particle⁶. At higher drives, the bulk pinning can counterintuitively lower the effective drag on the probe particle. This occurs since the drag originates when having a portion of the surrounding particles move with the probe particle, so that when the quenched disorder strongly immobilizes the surrounding particles, they can no longer move with the probe particle, leading to an effective decoupling of the probe particle from the surrounding media⁶. For probe particles driven through crystalline structures in the absence of quenched disorder, shear thinning¹ and directional locking effects occur where the amount of drag on the probe particle depends on the orientation of the drive with respect to the symmetry directions of the crystalline structure. Flow along a symmetry direction produces a lower drag since the probe particle can move easily between particles in the background lattice without constantly generating new topological defects, while for other driving directions, the probe particle induces the formation of local topological defects, leading to increased drag²⁵. It was also shown that for driving along symmetry directions, the drag in-

creases as the bulk melting temperature is approached due to the formation of topological defects in the region surrounding the probe particle, leading to a local melting transition⁴.

Here, instead of a single driven probe particle, we consider the case of a localized quasi-one-dimensional region of particles driven externally along a line. The drive is parallel to the orientation of the line. Such a geometry could be created using a laser beam directed along the sample edge, with magnetic particles driven by a magnetic strip, or with particles coupled to a mechanical external drive or driven with one-dimensional arrays of optical traps^{26–28}. Driven line geometries have already been realized for particles with Yukawa interactions in dusty plasmas, where a laser beam pushes particles only along a line^{29–33}. It is also possible to create systems with bulk pinning and an easy flow channel in confined geometries^{34–37}. A key difference between the point probe particle and the line probe considered here is that the line probe more directly mimics a shear response. If the system is strongly coupled, then an elastic response will occur in which the particles in the system move along with the particles in the driven line. Here we study the case of a line of particles driven along a symmetry direction of the background lattice for monodisperse ordered, bidisperse ordered, and bidisperse disordered systems, both for pin-free samples and for samples that have pinning present in the bulk.

II. SIMULATION AND SYSTEM

In Fig. 1 we illustrate the geometry of the sample, which consists of a two-dimensional assembly of N_c colloids with periodic boundary conditions in the x and y -directions. The arrows in the middle of Fig. 1 indicate the region within which the colloids experience an external drive $\mathbf{F}^D = F^D \hat{\mathbf{x}}$. Colloids outside this region are undriven and have $F^D = 0$. The colloid density is $\rho = N_c/L^2$, where L is the size of the simulation cell. The particles interact via a Yukawa or screened Coulomb potential. In some cases, we also consider the effect of pinning sites that we model as localized parabolic traps of radius r_p .

The dynamics of particle i arise from integrating the following equation of motion:

$$\eta \frac{d\mathbf{R}_i}{dt} = - \sum_{i \neq j}^{N_i} \nabla V(R_{ij}) + \mathbf{F}_i^P + \mathbf{F}_i^D + \mathbf{F}_i^T. \quad (1)$$

Here η is the damping constant, $\mathbf{R}_{i(j)}$ is the position of particle $i(j)$, and $R_{ij} = |\mathbf{R}_i - \mathbf{R}_j|$. The particle-particle interaction potential is $V(R_{ij}) = q^2 E_0 \exp(-\kappa R_{ij})/R_{ij}$. Here $E_0 = Z^{*2}/4\pi\epsilon\epsilon_0 a_0$, where q is the dimensionless interaction strength, Z^* is the effective charge of the colloid, ϵ is the solvent dielectric constant, and $1/\kappa$ is the screening length. Lengths are measured in units of a_0 , time in units of $\tau = \eta/E_0$, and forces in units of

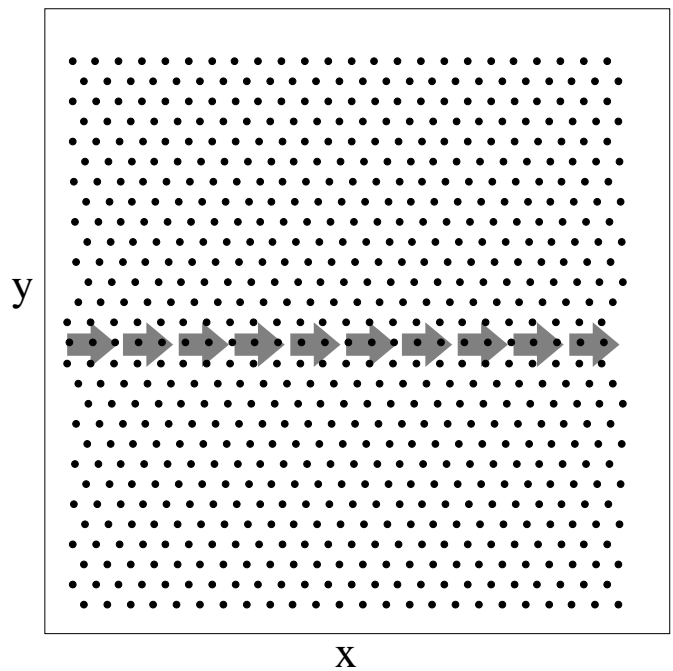


FIG. 1: Illustration of the sample geometry for the monodisperse case. Black dots: Colloids interacting via a pairwise Yukawa potential to form a triangular lattice. Arrows indicate the region within which an external drive in the positive x direction is applied to the particles. There are periodic boundary conditions in the x and y -directions.

$F_0 = E_0/a_0$. The driving force $\mathbf{F}^D = F_d \hat{\mathbf{x}}$ is applied only to particles in a region of width d at the center of the sample. We increase the external drive in increments of δF_D , then hold the drive at a constant value for a fixed period of time and measure the average velocity of the particles within the driven channel V_c and of the particles in the bulk V_b . The pinning force arises from N_p non-overlapping parabolic pinning sites that are placed outside the driven channel. The pinning force has the form $\mathbf{F}_i^P = F_p(R_{ik}/R_p)\Theta(R_p - R_{ik})\hat{\mathbf{R}}_{ik}$, where $R_{ik} = |\mathbf{R}_i - \mathbf{R}_k|$ is the distance between particle i and the center of pinning site k , and $\hat{\mathbf{R}}_{ik} = (\mathbf{R}_i - \mathbf{R}_k)/R_{ik}$. Here R_p is the pinning site radius, F_p is the maximum force of the pinning site, and Θ is the Heaviside step function. The effects of thermal fluctuations come from the Langevin noise term F^T with the properties $\langle F^T(t) \rangle = 0$ and $\langle F_i^T(t) F_j^T(t') \rangle = 2\eta k_B \delta_{ij} \delta(t - t')$, where k_B is the Boltzmann constant. The initial particle configurations are obtained by placing the colloids in a triangular arrangement, and unless otherwise noted, the average lattice constant is $a = 2.0$.

III. MONODISPERSE SYSTEM

In Fig. 2(a) we plot the average velocity of the particles in the driven channel region $\langle V_c \rangle$ versus external drive

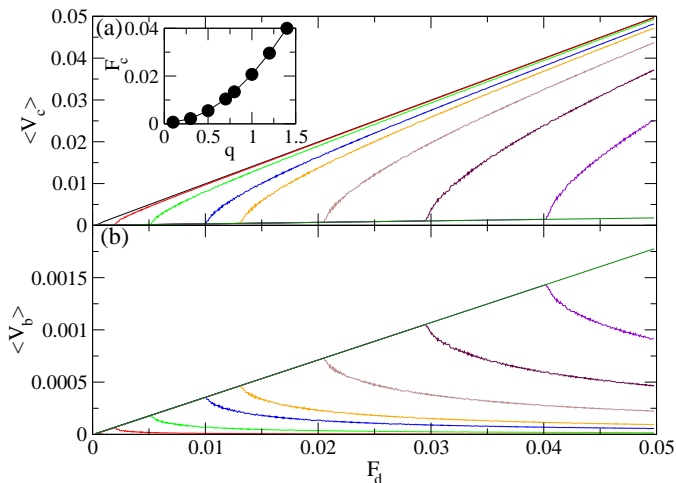


FIG. 2: A monodisperse system of colloids with varied interaction strength q and with $a = 2$. (a) The velocities of the particles in the driven channel region $\langle V_c \rangle$ vs F_d , where the velocities are normalized by the number of particles in the driven region. (b) The velocities of the particles in the bulk outside of the driven region $\langle V_b \rangle$ vs F_d , where the velocities are normalized by the number of particles in the non-driven region. The curves are for q values (from left to right) $q = 0.1, 0.3, 0.5, 0.7, 0.8, 1.0, 1.2, 1.4$, and 1.6 . There are two regimes. The first is an elastic region with $V_c = V_b$ where all the particles move together. This is followed at higher F_d by a decoupled regime where the particles in the driven line move past the bulk particles, while the bulk particles remain locked with each other. The inset in (a) shows that the driving force F_c at which the decoupling transition occurs increases with increasing q .

F_d , and in Fig. 2(b) we plot the corresponding average velocity of the particles outside of the driven channel, $\langle V_b \rangle$, versus F_d for a system with a monodisperse triangular crystalline arrangement of colloids. The different curves indicate the effect of changing the interaction coefficient q . For low F_d , all the curves for both $\langle V_c \rangle$ and $\langle V_b \rangle$ increase linearly and $\langle V_c \rangle = \langle V_b \rangle$, corresponding to the elastic flow regime where the particles in the driven region are locked with the bulk particles. Here there is no tearing or rearrangements, so all the particles keep their same neighbors and move together. At higher drives, a transition occurs to a regime where $\langle V_b \rangle$ decreases and $\langle V_c \rangle$ increases with increasing F_d . This occurs when the particles in the driven channel partially decouple from the bulk particles and are able to move past them. The bulk particles continue to move due to the coupling to the driven particles; however, as F_d increases, this coupling becomes weaker and $\langle V_b \rangle$ decreases. The inset in Fig. 2(a) shows the force F_c at which the decoupling occurs as a function of q . As the strength of the particle-particle interactions increases, a larger force must be applied before decoupling can occur.

The velocity-force curves in Fig. 2 are very similar to those found in other systems that exhibit decoupling and drag effects. One of the best known examples is the Gi-

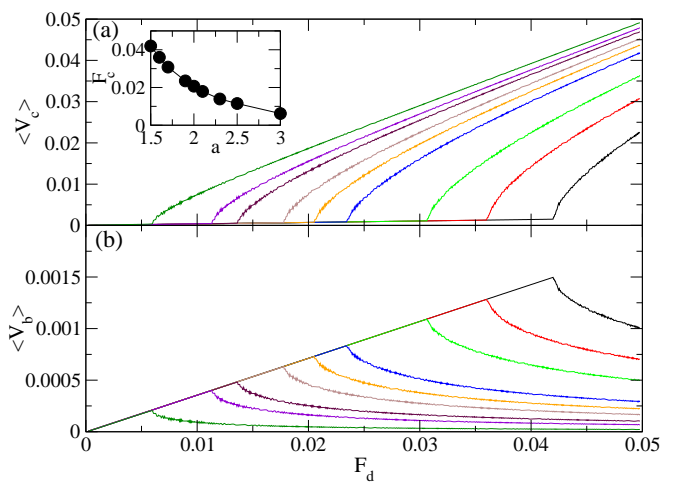


FIG. 3: A monodisperse system of colloids with $q = 1.0$ for varied colloid density. (a) $\langle V_c \rangle$ vs F_d . (b) $\langle V_b \rangle$ vs F_d . The colloid lattice constant $a = 3.0, 2.5, 2.3, 2.1, 2.0, 1.9, 1.7, 1.6$, and 1.5 , from left to right. Samples with larger a are less dense and decouple at a lower driving force. The inset in (a) shows F_c vs a .

aver transformer geometry for coupled superconducting layers in the presence of a magnetic field^{38,39}. Each quantized magnetic field line must pass through both layers, providing a magnetic coupling between the layers. When only one layer is driven by a current, the voltage response, which is proportional to the superconducting vortex velocity, is identical in both layers, indicating that the vortices in the two layers are locked together. As the drive increases, there is a decoupling transition between the layers associated with a decrease in the effective drag on the driven layer. This causes the velocity of the vortices in the driven layer to increase while the velocity of the vortices in the secondary or undriven layer drops. In this superconducting system, the interaction between vortices in neighboring layers is attractive, while in the colloidal system, the interactions between colloids in the driven and undriven regions are repulsive. The response of repulsively interacting particles in coupled one-dimensional wires has been studied for classical electrons⁴⁰ and particles with Yukawa interactions^{41,42}. In these systems, a commensurate state can form when the number of particles in each layer is the same, producing a well defined coupling-decoupling transition when one layer is driven. In the case of our driven line of particles, the system can be viewed as a single driven one-dimensional layer interacting with an array of non-driven layers. At the decoupling transition, the particles outside of the driven region remain locked together so that a very small shear band occurs only at the driven line. For more disordered systems, a much broader shear band forms.

In Fig. 3 we show $\langle V_c \rangle$ and $\langle V_b \rangle$ vs F_d for a monodisperse sample with fixed $q = 1.0$ but varied colloid density, measured in terms of the lattice constant a . The inset of Fig. 3(a) shows the dependence of the decou-

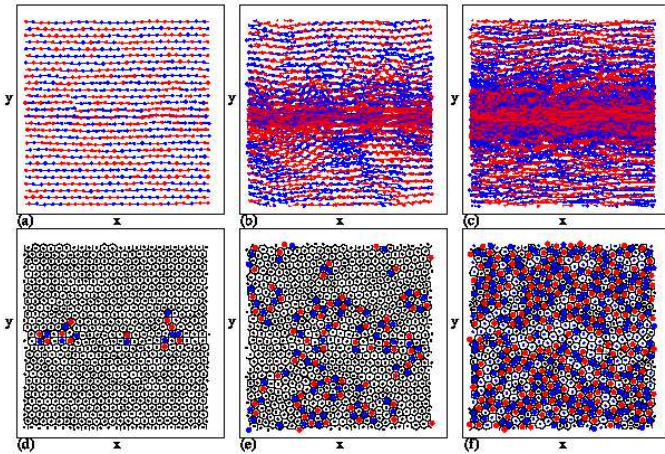


FIG. 4: A bidisperse colloidal system where half the particles have charge q_1 and the other half have charge $q_2 = 1.0$. (a,b,c) Dots: Particle positions. Dark (blue) particles have charge q_1 and light (red) particles have charge q_2 . Lines indicate the trajectories followed by the particles over a fixed time interval. (d,e,f) Voronoi construction. White polygons correspond to particles with six neighbors, dark blue polygons to particles with five neighbors, and light red polygons to particles with seven neighbors. (a,d) At $q_1/q_2 = 0.7$ and $F_d = 0.05$, the system is mostly ordered. There are some dislocations near the driven region due to the fact that the driven particles are moving faster than the bulk particles. These dislocations all have their Burgers vectors aligned in the same direction. (b,e) At $q_1/q_2 = 1.6$, the system is partially disordered in the bulk and there is a mixing of the trajectories as the shear band widens. (c,f) At $q_1/q_2 = 2.4$, the system is strongly disordered and the width of the shear band is increased.

pling force F_c on a . We observe a trend similar to that of changing q , where the samples with lower density have weaker particle-particle interactions and a lower decoupling threshold. The decoupling transition should also depend on the commensurability ratio of the particles in the driven channel with the surrounding media. If the density in the driven channel is higher or lower than that of the bulk, the decoupling force will be depressed relative to the case we consider here where the two densities are equal. This is a result of the localized incommensurations that separate the two regions of different densities. The incommensurations depin below the bulk decoupling transition and shift the transition to lower F_d . Studies of one-dimensional coupled channels also found that the decoupling transition drops to lower drives at incommensurate channel filling ratios⁴¹.

IV. BIDISPERSE SYSTEMS

We next consider a bidisperse system where half the particles have an interaction coefficient of q_1 and the other half have an interaction coefficient of q_2 . In Fig. 4(a,b,c) we plot the particle positions and trajectories during a fixed period of time, and in Fig. 4(d,e,f)

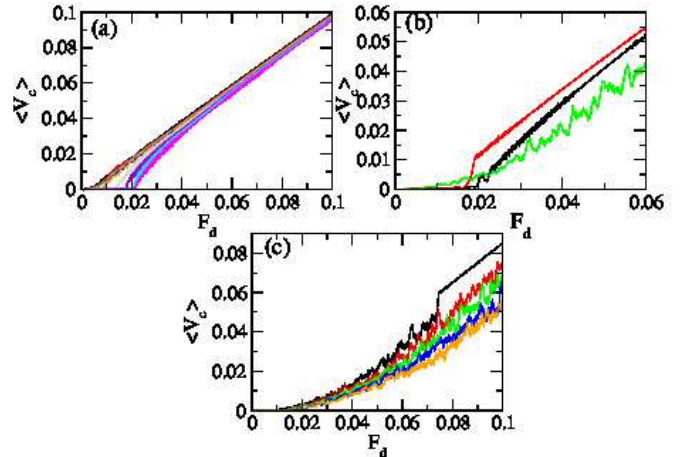


FIG. 5: $\langle V_c \rangle$ vs F_d for bidisperse systems with $q_2 = 1.0$. (a) $q_1/q_2 = 0.1, 0.2, 0.3, 0.5, 0.7, 0.8, 0.9, 1.0$, and 1.1 , from left to right. The system is disordered for $q_1/q_2 \leq 0.6$. (b) $q_1/q_2 = 1.3$ (center right), 1.4 (upper right), and 1.8 (lower right). F_c is highest for $q_1/q_2 = 1.3$ and lowest for $q_1/q_2 = 1.8$. The system is disordered for $q_1/q_2 = 1.8$, producing the enhanced fluctuations in the velocities. There is also a crossing of the velocity-force curves, where $\langle V_c \rangle$ at $q_1/q_2 = 1.8$ is lower in the moving phase than $\langle V_c \rangle$ of the ordered state due to the widened shear band in the moving state in the disordered system. (c) The disordered states at $q_1/q_2 = 2.2, 2.4, 2.6, 2.8$ and 3.0 , from top to bottom. Here $\langle V_c \rangle$ for fixed F_d decreases with increasing q_1/q_2 .

we show the Voronoi tessellations of the particle positions at one instant. For $q_1/q_2 = 0.7$ and $F_d = 0.05$, in Fig. 4(a,d), the system is crystalline with sixfold ordering in the bulk. The topological defects are concentrated near the driven line since the system is in the decoupled phase where the particles in the driven line move faster than the bulk particles. There is also no transverse diffusion in the system, as indicated by the nearly one-dimensional, non-mixing trajectories of the particles. In Fig. 4(b,e) at $q_1/q_2 = 1.6$, the bulk is disordered with a proliferation of 5-7 paired defects. The trajectories show that there is strong mixing near the driven line, with the most strongly disordered region concentrated near the driven line. Fig. 4(c,f) shows that for $q_1/q_2 = 2.4$, the system is even more disordered, and contains an increased number of 5-7 defects. In addition, the region of strong mixing, denoted by the region with crossing trajectories, is now wider in the y -direction. For $0.6 < q_1/q_2 < 1.6$, the bulk is ordered. For $q_1/q_2 < 0.6$ the system disorders and the trajectories are similar to those shown in Fig. 4(b).

The different phases can also be identified via changes in the features of the velocity-force curves. In Fig. 5(a) we plot $\langle V_c \rangle$ vs F_D for samples with $q_1/q_2 = 0.1$ to 1.1 . As q_1/q_2 increases, the decoupling force F_c increases. The concavity of the velocity-force curves can be fit to $\langle V_c \rangle \propto (F - F_c)^\beta$, where $\beta > 1.0$ for the disordered systems with $q_1/q_2 \leq 0.6$ and $\beta < 1.0$ in the

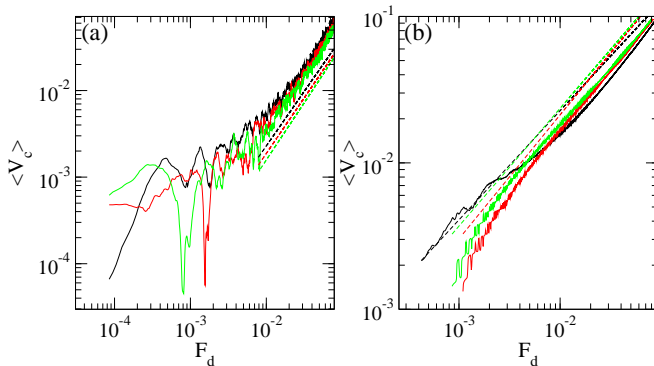


FIG. 6: (a) $\langle V_b \rangle$ vs $F_d - F_c$ for a bidisperse system with $q_2 = 1.0$, where F_c is the force at decoupling or depinning. (a) $q_1/q_2 = 2.6, 2.8$, and 3.0 , from top right to bottom right. The dashed lines are power law fits (vertically offset for clarity) with exponents of $\beta = 1.26, 1.29$, and 1.32 , respectively. (b) The same for the ordered regime of $q_1 = 0.7, 0.9$, and 1.0 , from bottom right to top right, with dashed lines indicating power law fits (vertically offset for clarity) of $\beta = 0.746, 0.84$, and 0.8 , respectively.

ordered systems. This is shown more clearly in Fig. 5(b) where we plot $\langle V_c \rangle$ vs F_d for systems with $q_1/q_2 = 1.3, 1.4$, and 1.8 . For the disordered case of $q_1/q_2 = 1.8$, there are stronger fluctuations in $\langle V_c \rangle$. F_c is highest for $q_1/q_2 = 1.3$ but is lower in the disordered regime for $q_1/q_2 = 1.8$. A crossing of the velocity-force curves occurs since F_c for the $q_1/q_2 = 1.8$ system is lower than for the $q_1/q_2 = 1.3$ system, but at higher drives $\langle V_c \rangle$ is lower in the $q_1/q_2 = 1.8$ sample. This occurs since the ordered state at $q_1/q_2 = 1.3$ produces a sharp shear band, while the disordered state at $q_1/q_2 = 1.8$ has a wide shear band region similar to that illustrated in Fig. 4(b), meaning that more particles are being dragged by the line particles, causing the driven particles to move more slowly.

Figure 5(c) shows $\langle V_c \rangle$ versus F_D for $2.2 \leq q_1/q_2 \leq 3.0$, where the system remains disordered with large fluctuations in $\langle V_c \rangle$. For a fixed drive, $\langle V_c \rangle$ drops with increasing q_1/q_2 . Here the velocity-force curves can be fit to the form $\langle V_c \rangle - V_{dc} \propto (F_d - F_c)^\beta$ with $\beta \approx 1.3$, where V_{dc} is the velocity at F_c . This fit is illustrated in Fig. 6(a) for $q_1/q_2 = 2.6, 2.8$, and 3.0 . A power law fit of this type is similar to that observed for a single particle moving through a disordered medium when the driven particle creates a large amount of distortion, including particle rearrangements^{2,43}. Similar scaling is found at depinning for assemblies of particles that undergo plastic flow upon depinning; such tearing behavior generates an exponent ranging from $\beta = 1.25$ to $\beta = 2.0$ ^{20,44}. Near an elastic depinning transition, the velocity-force curve can also be fit with a power law but with a smaller exponent $\beta < 1.0$ ^{44,45}. For samples in the ordered regime, we can fit $\langle V_c \rangle - V_{dc}$ to a similar scaling form with $\beta \approx 0.8$, as shown in Fig. 6(b) for $q_1/q_2 = 0.7, 0.9$, and 1.0 . This indicates that the decoupling transition in the ordered phase

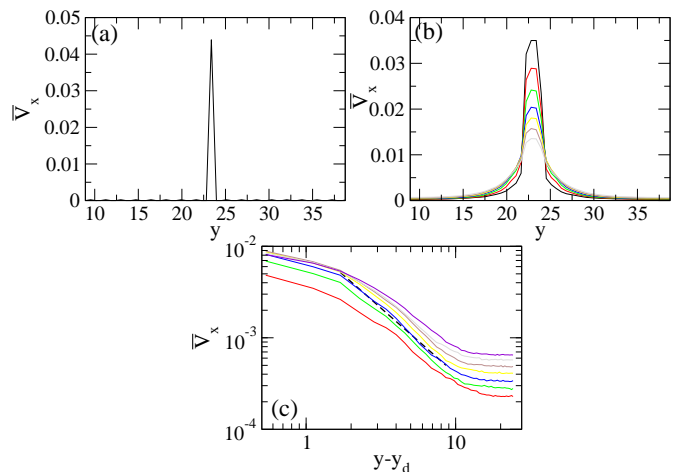


FIG. 7: (a,b) Velocity profiles \bar{V}_x vs y for a bidisperse system with $q_2 = 1.0$. The driven region is centered at $y_d = 23$. (a) In a sample with $q_1/q_2 = 1.0$ at $F_d = 1.0$, a sharp shear band forms. (b) Samples with $q_1/q_2 = 1.8, 2.0, 2.2, 2.4, 2.6, 2.8$, and 3.0 , from top center to bottom center. \bar{V}_x in the driven region drops with increasing q_1/q_2 , while \bar{V}_x in the bulk increases with increasing q_1/q_2 as the shear band widens. (c) \bar{V}_x in only the top half of the sample vs $y - y_d$ for samples with $q_1/q_2 = 1.8, 2.2, 2.4, 2.6, 2.8$, and 3.0 , from top to bottom. Dotted line is a power law fit for the $q_1/q_2 = 2.2$ system with an exponent of -1.4 in the region of strong mixing. At large $y - y_d$, the bulk becomes locked again and moves as a solid.

resembles the elastic depinning of a one-dimensional coupled chain of particles from a periodic substrate created by the periodic ordering of the bulk particles. We find similar scalings for the other fillings we have considered, where for the ordered systems $\beta < 1.0$ and for the disordered systems $\beta > 1.0$.

The shear banding effect can be better seen by examining profiles of the average x velocity \bar{V}_x taken at different points along the y -direction. Here, $\bar{V}_x(y) = \sum_{i=1}^{N_c} (\hat{\mathbf{R}}_i \cdot \hat{\mathbf{x}}) [\Theta(R_y^i - y - \delta y/2) \Theta(y + \delta y/2 - R_y^i)]$ where R_y^i is the y coordinate of particle i and δy is the width of the averaging region. Figure 7(a) shows the velocity profiles $\bar{V}_x(y)$ for $q_1/q_2 = 1.0$ at $F_d = 1.0$. A sharp spike in \bar{V}_x appears at $y = y_d$, the center of the driven region, while $\bar{V}_x \approx 0$ in the bulk undriven portion of the sample. This type of profile is observed for all samples where the system remains ordered in the decoupled phase. In Fig. 7(b) we plot $\bar{V}_x(y)$ for disordered samples with $q_1/q_2 = 1.8, 2.0, 2.2, 2.4, 2.6, 2.8$, and 3.0 . In all cases, \bar{V}_x is maximum at $y = y_d$ and falls off for larger $|y - y_d|$. As q_1/q_2 increases, \bar{V}_x at $y = y_d$ decreases while in the bulk \bar{V}_x increases. This coincides with the decrease in $\langle V_c \rangle$ for increasing q_1/q_2 shown in Fig. 5(c). The increase of the response in the bulk occurs when a larger number of particles are dragged by the driven line due to the increased particle-particle interaction strength. In Fig. 7(c) we plot \bar{V}_x for only the upper half of the sample versus $y - y_d$ on

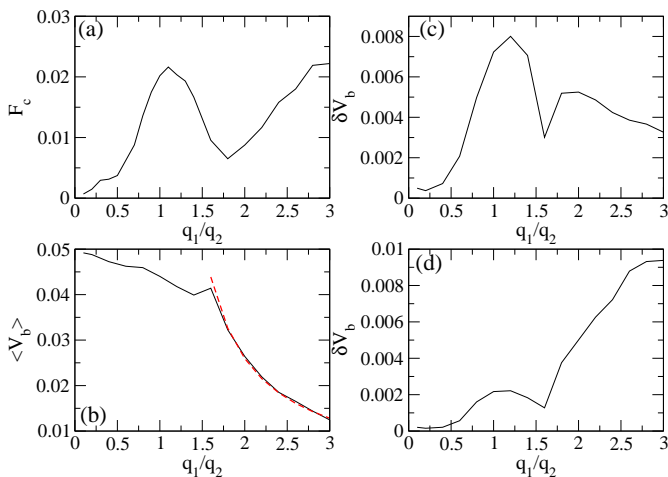


FIG. 8: A bidisperse sample with $q_2 = 1.0$. (a) F_c vs q_1/q_2 . A peak appears in the ordered region centered close to $q_1/q_2 = 1.0$. (b) $\langle V_b \rangle$ vs q_1/q_2 at $F_d = 0.05$. The velocity drops in the disordered regime $q_1/q_2 \geq 1.6$. The dashed line indicates a fit to $1/(q_1/q_2)$ in the disordered regime. (c) The standard deviation of the fluctuations in the bulk velocity δV_b vs q_1/q_2 for $F_d = 0.05$. (d) δV_b vs q_1/q_2 for $F_d = 0.1$.

a log-log scale, to better show where the shear banding is occurring. The dashed line in Fig. 7(c) is a power law fit to the data from the $q_1/q_2 = 2.2$ sample in the shear band region, and has an exponent of -1.4 . From the trajectory images in Fig. 4(c), it is clear that there is a region of strong mixing near the driven line and a region of less mixing at larger values of $y - y_d$, correlated with a saturation of \bar{V}_x in Fig. 7(c). As q_1/q_2 increases, the saturation region shifts out to larger values of $y - y_d$. This results shows that the system has liquid-like behavior near the shear band region, but acts more like a disordered elastic solid away from the driven region.

We summarize the behavior of F_c vs q_1/q_2 for the bidisperse samples in Fig. 8(a). In the disordered regime $0.1 < q_1/q_2 \leq 0.6$, F_c increases with increasing q_1/q_2 . Above $q_1/q_2 = 0.6$, when the system enters the ordered regime, F_c increases more rapidly and the crystalline order that appears near $q_1/q_2 = 1.0$ enhances the coupling transition, as indicated by the peak in F_c near $q_1/q_2 = 1.0$. As the system becomes disordered away from $q_1/q_2 = 1.0$, weak or defected spots appear that lower the decoupling transition and reduce F_c . A minimum in F_c appears near $q_1/q_2 = 1.8$ in the disordered region, while F_c increases again for larger q_1/q_2 due to the increasing strength of the particle-particle interactions, which also cause the system to depin plastically. The inset of Fig. 2(a) shows that F_c in the monodisperse system also increases with increasing q .

In Fig. 8(b) we plot $\langle V_b \rangle$ vs q_1/q_2 in the bidisperse samples at $F_d = 0.05$. Here the bulk velocity decreases at a moderate rate with increasing q_1/q_2 until the system becomes disordered for $q_1/q_2 \geq 1.6$ and large shear bands form, leading to a more rapid drop in $\langle V_b \rangle$ with

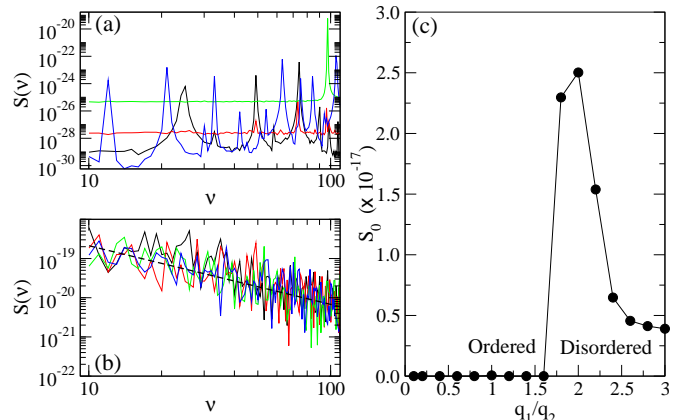


FIG. 9: (a,b) Power spectra $S(\nu)$ for bidisperse samples with $q_2 = 1.0$ at $F_d = 0.05$. (a) In ordered systems, $q_1/q_2 = 0.6$ (black), 0.8 (red), 1.0 (green), and 1.4 (blue), there is a narrow band noise signature. (b) In disordered systems, $q_1/q_2 = 2.4$ (black), 2.6 (red), 2.8 (green), and 3.0 (blue), a broad band noise signal occurs. The dashed line is a power law fit with an exponent of -1.5 . (c) The noise power S_0 vs q_1/q_2 . At the transition into the disordered regime, S_0 jumps to a much higher value.

increasing q_1/q_2 . The dashed line is a fit to $1/(q_1/q_2)$ in the disordered regime. Just before the system disorders, for $1.4 \leq q_1/q_2 < 1.6$, there is a slight increase in $\langle V_b \rangle$ that is correlated with a drop in the standard deviation of the velocity fluctuations δV_b , as shown in Fig. 8(c). For $F_d = 0.05$, Fig. 8(c) indicates that δV_b reaches a maximum for $q_1/q_2 = 1.1$, the same value at which there is a peak in F_c in Fig. 8(a). At this point, when the velocity oscillations are the largest, the particles are moving in a one-dimensional ordered pattern and each particle exhibits an oscillating velocity component due to the effective periodic potential created by the ordered particles in the bulk. There is a dip in δV_b at the transition from the ordered to the disordered region at $q_1/q_2 = 1.6$; for $q_1/q_2 > 1.6$, δV_b decreases with increasing q_1/q_2 . At the disordering transition, the particles no longer move together but have different sliding velocities, resulting in a cancellation of the large oscillations that appeared in the ordered phase. For larger q_1/q_2 , deeper into the disordered regime, the velocity fluctuations decrease with increasing q_1/q_2 due to a decrease in the amount of motion in the system as the fixed value of F_d gets closer to F_c , which increases with increasing q_1/q_2 . At $F_d = 0.1$, Fig. 8(d) shows that the same general trends in δV_b persist; however, in this case the velocity fluctuations for larger q_1/q_2 increase with increasing q_1 since the higher drive causes a large shear banding effect. There is a saturation of δV_b near $q_1/q_2 = 3.0$, and we expect that the velocity fluctuations will decrease for higher q_1/q_2 as F_c increases and approaches the fixed value $F_d = 0.1$. These results indicate that the order-disorder transition can be detected by measuring the velocity fluctuations.

The velocity fluctuations can also be characterized us-

ing the power spectrum $S(\nu) = |\int V_b(t)e^{-2\pi i\nu t} dt|^2$. In the ordered regime, the noise fluctuations have a narrow band noise feature indicating that there is a characteristic frequency. Similar narrow band noise occurs for particles moving over a periodic substrate, where the characteristic frequency is determined by the rate at which the particle travels from one substrate minimum to the next⁴⁶. In Fig. 9(a) we plot $S(\nu)$ in the ordered regime for samples with $q_1/q_2 = 0.6, 0.8, 1.0,$ and 1.4 for a fixed drive of $F_d = 0.05$. The peaks in the spectra indicate the presence of narrow band noise. In the disordered regime, we find broad band noise or a $1/f^\alpha$ noise signature, as shown in Fig. 9(b) for $q_1/q_2 = 2.4, 2.6, 2.8,$ and 3.0 . Here $\alpha = -1.5$. Similar broad band noise has been observed for dragging a single particle through granular media at the jamming transition⁶ and for plastic depinning of particles on disordered substrates⁴⁷. We can also analyze the noise power $S_0 = \int_{\nu_1}^{\nu_2} S(\nu)$ for a fixed octave, as shown in Fig. 9(c) for $\nu_1 = 10$ and $\nu_2 = 100$. Here S_0 is small in the ordered regime $0.6 < q_1/q_2 < 1.6$ and undergoes a pronounced increase to a maximum near the onset of the disordered regime. For $q_1/q_2 \leq 0.6$, the system is also disordered and $S(\nu)$ shows broad band noise; however, the noise power remains very low for these small values of q_1/q_2 .

A. Dynamic phases

For bidisperse samples with large q_1/q_2 , we find an additional dynamical phase at high drives where the shear band region becomes strongly localized again and the bulk particles lock together, similar to the behavior found in the ordered regime. In Fig. 10(a) we plot $\langle V_c \rangle$ versus F_d for a bidisperse sample with $q_1/q_2 = 1.6$. For low F_d , the system is crystalline and strongly coupled, so that all the particles move together. As F_d increases, the system becomes disordered and produces a large shear band (illustrated in Fig. 10(c) for $F_d = 0.05$) associated with large velocity fluctuations. At higher drives, however, there is a transition to a strongly shear localized state where only a single line of particles are moving while the bulk particles lock together and moving at a very slow velocity, as shown in Fig. 10(d) for $F_d = 0.09$. The onset of this phase is accompanied by a drop in the velocity fluctuations in Fig. 10(a). In Fig. 10(b) we plot $\langle V_b \rangle$ versus F_d for the same system, showing that at the shear localization transition, the bulk velocity drops to a value slightly above zero. At the transition, $\langle V_c \rangle$ increases since the drag from the bulk particles on the particles in the driven channel is reduced. The shear localization occurs when the particles in the driven line are moving sufficiently rapidly that they can no longer couple effectively to the bulk particles. This transition is a general feature that occurs in the disordered state. Since the transition is dominated by fluctuations, the drive at which it occurs can vary significantly from one sample realization to another; however, on average the transition occurs at

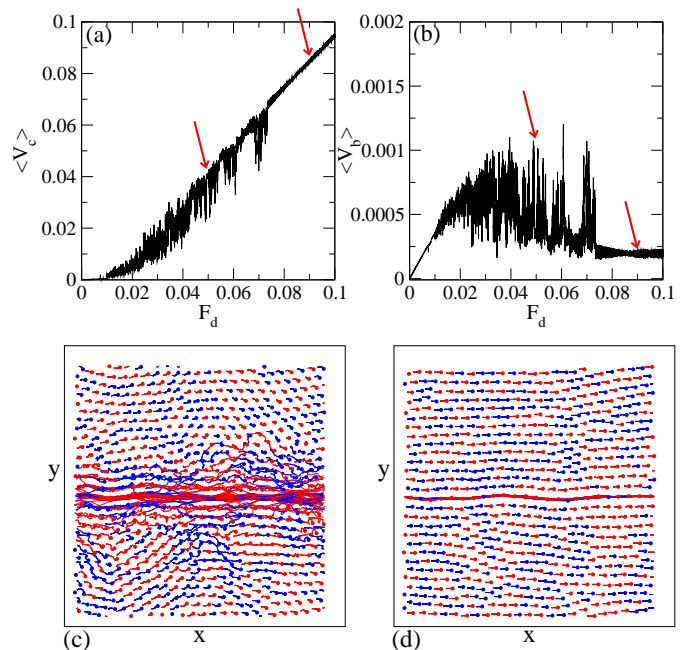


FIG. 10: (a) $\langle V_c \rangle$ vs F_d for a bidisperse system with $q_1/q_2 = 1.6$ and $q_2 = 1.0$. At low drives, the system is crystalline and moves as a solid unit. At decoupling, the system enters a disordered regime, while at higher drives $F_d > 0.075$, there is a transition to a state with strongly localized shear and reduced velocity fluctuations. (b) $\langle V_b \rangle$ vs F_d for the same system. The bulk velocity drops almost to zero at the onset of the shear localization transition. (c,d) Particle positions (filled circles) and trajectories (lines) in the same system for (c) the disordered decoupled state at $F_d = 0.05$ and (d) the strongly localized shear state at $F_d = 0.09$. Arrows in (a) and (b) indicate the drives at which the images in (c) and (d) were obtained.

higher values of F_d for increasing q_1/q_2 or decreasing a . The shear localized state has small velocity fluctuations with low noise that is white ($\alpha = 0$).

V. QUENCHED DISORDER AND SHEAR LOCALIZATION

We next examine the effects of adding quenched disorder or pinning sites in the bulk region. In Fig. 11 we plot the particle trajectories in the disordered regime for a bidisperse sample with $q_1/q_2 = 1.8$ at $F_d = 0.05$. The pinning sites are placed an average distance d_p from the driven region. Each pin captures a single colloid and the pinning force is sufficiently strong that the particles do not depin over the range of F_d we consider. The repulsive nature of the particle-particle interactions prevents unpinned particles from closely approaching pinned particles, leading to a reduction in the density of particle trajectories in the vicinity of each pinned particle. For a small number of pinning sites $N_p = 4$, shown in Fig. 11(a) for a sample with $d_p = 3a$, the overall particle trajectories

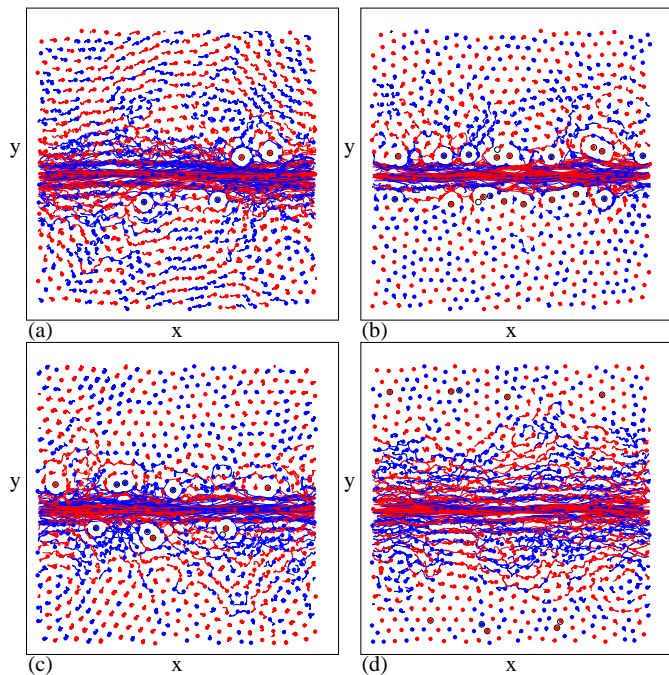


FIG. 11: The particle positions (filled circles) and trajectories (lines) at a constant drive of $F_d = 0.05$ for a bidisperse system at $q_1/q_2 = 1.8$ and $q_2 = 1.0$ with quenched disorder added in the form of localized pinning sites placed at an average distance of d_p from the driven line. The open circles are the locations of the pinning sites that each capture one colloid. (a) $N_p = 4$ and $d_p = 3a$. (b) $N_p = 20$ and $d_p = 3a$. As the number of pinning sites increases, the flow becomes more localized. (c) $N_p = 10$ and $d_p = 2a$. (d) $N_p = 10$ and $d_p = 18a$.

do not differ significantly from the pin-free system; however, as the number of pinning sites increases, the mixing region surrounding the driven line is reduced in width, as illustrated in Fig. 11(b) for a sample with $N_p = 20$ and $d_p = 3a$. Here, there is no longer any net motion of the bulk particles, indicating a complete screening of the shear banding effect by the pinning. This result shows that quenched disorder can produce strong shear localization.

In Fig. 12(a) we plot $\langle V_c \rangle$ versus F_d for a bidisperse pinned system with $q_1/q_2 = 1.8$, $N_p = 16$, and $d_p = 2a$ where we observe a pinned regime, a coupled disordered flow regime, and a decoupled regime for high drive similar to that found for the pin-free system in Fig. 10. In the absence of pinning, at low drives the particles all move as a locked solid; however, when pinning is added to the system, there is a true pinned phase at low drive where particle motion does not occur. In Fig. 12(b) we plot the dynamic phase diagram for F_d versus the number of pinning sites N_p . The transitions between the different phases show strong fluctuations from one realization to another, and in Fig. 12(b) we show the transition line averaged over several different disorder realizations. The transition between the coupled and decoupled regimes

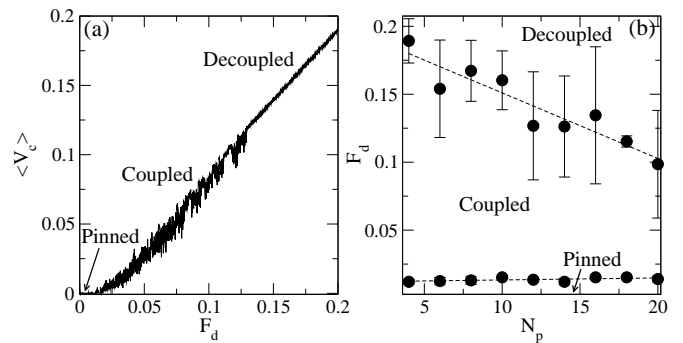


FIG. 12: (a) $\langle V_c \rangle$ vs F_d for a bidisperse system at $q_1/q_2 = 1.8$ and $q_2 = 1.0$ with quenched disorder where $N_p = 16$ and $d_p = 2a$. The pinned, coupled disordered, and high drive decoupled regimes are labeled. (b) Dynamic phase diagram for F_d vs N_p in bidisperse samples with $q_1/q_2 = 1.8$. The pinned, coupled disordered, and high drive decoupled regimes are labeled. As N_p increases, the transition between the coupled and decoupled phases drops to lower values of F_d .

drops to lower F_d with increasing N_p . For a fixed drive, we find the interesting effect that the onset of the decoupled regime is correlated with an increase in the velocity of the particles in the driven line. Thus, by increasing the number of pinning sites, it is possible to cause the driven particles to move at a higher velocity. This effect arises due to the effective screening of the driven particles from the bulk particles by the pinned particles. A similar effect was observed for driving a single particle through a background of other particles and pinning sites, where for high drives, a decoupling transition between the driven and background particles leads to an increase in the velocity of the driven particle. In Fig. 11(c,d) we show the particle positions and trajectories for samples where the number of pinning sites is fixed at $N_p = 10$ for different pin spacings of $d_p = 2a$ [Fig. 11(c)] and $d_p = 18a$ [Fig. 11(d)]. Here the motion is more localized for the smaller value of d_p .

In Fig. 13(a) we show $\bar{V}_x(y)$ for bidisperse samples with $q_1/q_2 = 1.8$, $d_p = 2a$, and $F_d = 0.024$ for different numbers of pinning sites ranging from $N_p = 0$ to $N_p = 20$. For the pin-free system with $N_p = 0$, \bar{V}_x far from the driven line reaches a finite value since all of the particles in the system move. As the number of pinning sites increases, \bar{V}_x decreases at all length scales, with \bar{V}_x in the driven line region decreasing more slowly than \bar{V}_x in the region far from the driven line. For a sufficiently large number of pinning sites, \bar{V}_x drops to zero for distances of $6a$ or greater away from the driven line, indicating a complete screening of the shear band by the pinned particles. In Fig. 13(b) we show \bar{V}_x for the same system with fixed $N_p = 10$ and varied d_p . For increasing d_p , \bar{V}_x in the bulk gradually increases.

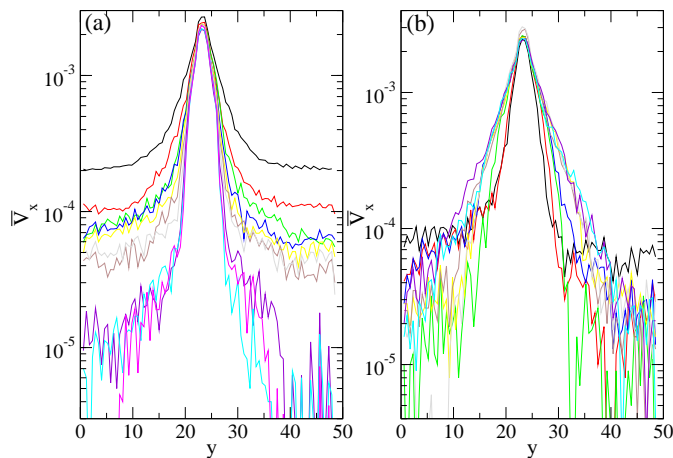


FIG. 13: Velocity profiles \bar{V}_x vs y for bidisperse samples with $q_1/q_2 = 1.8$ and $q_2 = 1.0$ at $F_d = 0.024$. (a) $d_p = 2a$ and $N_p = 0, 4, 6, 8, 10, 12, 14, 16, 18,$ and 20 , from top center to bottom center. Here \bar{V}_x drops with increasing N_p at all length scales. (b) $N_p = 10$ and $d_p = 2a, 4a, 6a, 8a, 10a, 12a, 14a, 16a,$ and $18a$, from bottom center to top center. For the smallest d_p , the shear band is strongly localized.

VI. THERMAL EFFECTS

To study thermal effects, we focus on the monodisperse system with $q_1/q_2 = 1.0$ under fixed drive $F_d = 0.05$, which forms a crystalline state. In Fig. 14 we plot the particle positions and trajectories as well as Voronoi constructions of snapshots of the particle positions for increasing T . For low temperatures $T < 0.6$, the system remains ordered and the particle trajectories are one-dimensional. At $T = 0.6$, Fig. 14(a,d) shows that the trajectories near the driven line begin to mix, producing 5-7 paired defects, while the bulk particles remain ordered. At $T = 1.2$ in Fig. 14(b,e), the number of 5-7 defect pairs has increased and some pairs begin to migrate from the driven line into the bulk region, although the bulk remains mostly ordered. For $T = 1.56$ the bulk begins to disorder and a widened shear band appears. Figure 14(c,f) shows that at $T = 1.8$ the bulk is strongly disordered.

In Fig. 15(a), the plot of $\langle V_c \rangle$ versus T shows that the velocity drops when the dislocations begin to migrate out from the driven line region. There is a minimum in $\langle V_c \rangle$ at the bulk melting temperature. Figure 15(b) shows the corresponding fraction of six-fold coordinated particles, $P_6 = \sum_{i=1}^{N_c} \delta(z_i - 6)$, where z_i is the coordination number of particle i . For a perfect triangular lattice, $P_6 = 1.0$. We find that the drop in P_6 , indicating bulk melting, occurs at a higher temperature than the drop in $\langle V_c \rangle$. In previous numerical studies of single driven probe particles moving through a crystalline background, it was also found that the velocity drops when local dislocations near the driven probe particle occur, which typically begins for temperatures below the bulk melting temperature⁴.

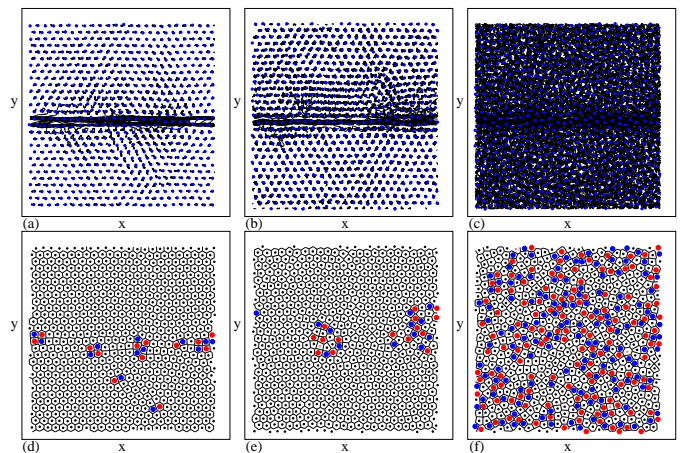


FIG. 14: A monodisperse pin-free system with $q_1/q_2 = 1.0$, $q_2 = 1.0$, and $F_d = 0.05$ at different temperatures. (a,b,c) Dots: Particle positions. Lines: the trajectories followed by the particles over a fixed time interval. (d,e,f) Voronoi construction. White polygons correspond to particles with six neighbors, dark blue polygons to particles with five neighbors, and light red polygons to particles with seven neighbors. (a,d) $T = 0.6$. The dislocations are primarily located along the driven line with their Burgers vectors aligned in the same direction. (b,e) $T = 1.2$. The dislocations have begun to migrate into the bulk. (c,f) $T = 1.8$, above the bulk melting temperature. The flow is disordered and topological defects have proliferated.

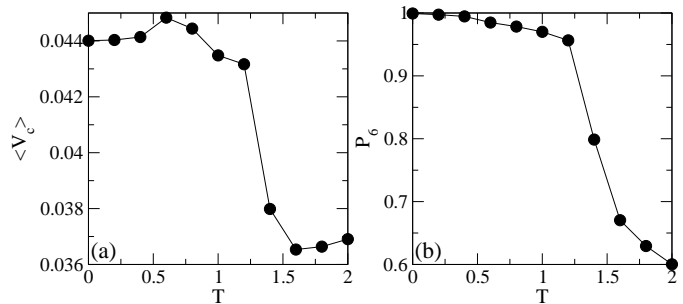


FIG. 15: (a) $\langle V_c \rangle$ vs T for a pin-free monodisperse system with $q_1/q_2 = 1.0$ and $q_2 = 1.0$ at $F_d = 0.05$. (b) The fraction of six-fold coordinated particles P_6 vs T . The system melts near $T = 1.5$ and the velocity of the particles in the driven line drops at temperatures just below the bulk melting transition.

At much higher temperatures, the velocities gradually increase again. This result shows that the driven line geometry can also be used to examine thermal melting properties.

VII. SUMMARY

We study the effects of driving a quasi-one-dimensional region of particles through a two-dimensional system of Yukawa interacting particles. In a monodisperse system

a crystalline state forms, and as a function of increasing external drive there is a well defined transition from elastic flow, where all the particles move together, to a decoupled flow, where the particles in the driven region decouple from the bulk particles and the bulk particles remain in a locked crystalline state. The properties of this elastic to decoupled transition are similar to those found in studies of layered systems where only one layer is driven and the other layer is dragged, such as a transformer geometry for bilayer superconductors or bilayer Wigner crystals. For bidisperse systems, the bulk becomes disordered, and the driven line produces a local shear band and velocity gradient. The bulk particles near the driven line can be dragged with the driven particles, and the average velocity of the particles in the driven line decreases as the width of the shear band region increases. In the disordered regime, for increasing drive we identify another decoupling transition where the bulk particles become locked, producing an elastic disordered solid, coinciding with the shear band becoming very sharp. We show how the decoupling force, noise fluctuations, and average velocities can be correlated with bulk disordering transitions. We also consider the effects of adding

quenched disorder or pinning, and find that the shear band region becomes increasingly localized for increasing pinning density. This results in an interesting effect where the velocity of the driven particles can be increased by adding more pinning sites to the system. Such systems could be realized experimentally using colloids or dusty plasmas with an optical drive applied along a one-dimensional channel, such as a laser applied along the edge of the sample. Variations of this geometry could also be constructed in superconducting vortex systems by embedding a single weak pinning channel in a bulk sample.

Acknowledgments

This work was carried out under the auspices of the NNSA of the U.S. DoE at LANL under Contract No. DE-AC52-06NA25396. The work of A. Libál was supported by a grant of the Romanian National Authority for Scientific Research, CNCS-UEFISCDI, project number PN-II-RU-TE-2011-3-0114.

-
- ¹ R.P.A. Dullens and C. Bechinger, Phys. Rev. Lett. **107**, 138301 (2011).
- ² P. Habdas, D. Schaar, A.C. Levitt, and E.R. Weeks, Europhys. Lett. **67**, 477 (2004).
- ³ I. Gazuz, A.M. Puertas, Th. Voigtmann, and M. Fuchs, Phys. Rev. Lett. **102**, 248302 (2009); M.V. Gnann, I. Gazuz, A.M. Puertas, M. Fuchs, and Th. Voigtmann, Soft Matter **7**, 1390 (2011).
- ⁴ C. Reichhardt and C.J. Olson Reichhardt, Phys. Rev. Lett. **92**, 108301 (2004).
- ⁵ C. Gutsche *et al.*, J. Phys.: Condens. Matt. **23**, 184114 (2011).
- ⁶ C.J. Olson Reichhardt and C. Reichhardt, Phys. Rev. E **78**, 011402 (2008).
- ⁷ H.H. Wensink and H. Löwen, Phys. Rev. Lett. **97**, 038303 (2006).
- ⁸ C. Reichhardt and C.J. Olson Reichhardt, Phys. Rev. Lett. **96**, 028301 (2006).
- ⁹ A.S. Khair and T.M. Squires, Phys. Rev. Lett. **105**, 156001 (2010).
- ¹⁰ R.L. Jack, D. Kelsey, J.P. Garrahan, and D. Chandler, Phys. Rev. E **78**, 011506 (2008).
- ¹¹ S.J. Gerbode, D.C. Ong, C.M. Liddell, and I. Cohen, Phys. Rev. E **82**, 041404 (2010).
- ¹² L.G. Wilson, A.W. Harrison, W.C.K. Poon, and A.M. Puertas, EPL **93**, 58007 (2011); L.G. Wilson and W.C.K. Poon, Phys. Chem. Chem. Phys. **13**, 10617 (2011).
- ¹³ D. Winter, J. Horbach, P. Virnau, and K. Binder, Phys. Rev. Lett. **108**, 028303 (2012).
- ¹⁴ C. Mejía-Monasterio and G. Oshanin, Soft Matter **7**, 993 (2011).
- ¹⁵ J.A. Drocco, M.B. Hastings, C.J. Olson Reichhardt, and C. Reichhardt, Phys. Rev. Lett. **95**, 088001 (2005).
- ¹⁶ R. Candelier and O. Dauchot, Phys. Rev. E **81**, 011304 (2010).
- ¹⁷ A. Fiege, M. Grob, and A. Zippelius, Gran. Matt. **14**, 247 (2012).
- ¹⁸ R. Harich, T. Darnige, E. Kolb, and E. Clement, EPL **96**, 54003 (2011).
- ¹⁹ C.J. Olson Reichhardt and C. Reichhardt, Phys. Rev. E **82**, 051306 (2010).
- ²⁰ S. Bhattacharya and M.J. Higgins, Phys. Rev. Lett. **70**, 2617 (1993); Y. Fily, E. Olive, N. Di Scala, and J.C. Soret, Phys. Rev. B **82**, 134519 (2010).
- ²¹ L. Luan, O.M. Auslaender, D.A. Bonn, R. Liang, W.N. Hardy, and K.A. Moler, Phys. Rev. B **79**, 214530 (2009).
- ²² O.M. Auslaender *et al.*, Nature Phys. **5**, 35 (2009).
- ²³ C. Reichhardt, Nature Phys. **5**, 15 (2009).
- ²⁴ E.W.J. Staver, J.E. Hoffman, O.M. Auslaender, D. Rugar, and K.A. Moler, Appl. Phys. Lett. **93**, 172514 (2008).
- ²⁵ C. Reichhardt and C.J. Olson Reichhardt, Phys. Rev. E. **69**, 041405 (2004).
- ²⁶ D. McGloin, A.E. Carruthers, K. Dholakia, and E.M. Wright, Phys. Rev. E **69**, 021403 (2004).
- ²⁷ C. Lutz, M. Kollmann, and C. Bechinger, Phys. Rev. Lett. **93**, 026001 (2004).
- ²⁸ Y. Roichman, D.G. Grier, and G. Zaslavsky, Phys. Rev. E **75**, 020401(R) (2007).
- ²⁹ Y. Feng, J. Goree, B. Liu, Phys. Rev. Lett. **104**, 165003 (2010).
- ³⁰ S. Nunomura, D. Samsonov, and J. Goree, Phys. Rev. Lett. **84**, 5141 (2000).
- ³¹ W.-T. Juan, M.-H. Chen, and L. I, Phys. Rev. E **64**, 016402 (2001); C.-W. Io and L. I, Phys. Rev. E **80**, 036401 (2009).
- ³² V. Nosenko and J. Goree, Phys. Rev. Lett. **93**, 155004 (2004).
- ³³ V. Nosenko, A.V. Ivlev, and G.E Morfill, Phys. Rev. Lett.

- 108**, 135005 (2012).
- ³⁴ M. Köppl, P. Henseler, A. Erbe, P. Nielaba, and P. Leiderer, *Phys. Rev. Lett.* **97**, 208302 (2006).
- ³⁵ B. Liu, K. Avinash, and J. Goree, *Phys. Rev. Lett.* **91**, 255003 (2003).
- ³⁶ N. Kokubo, R. Besseling, V.M. Vinokur, and P.H. Kes, *Phys. Rev. Lett.* **88**, 247004 (2002).
- ³⁷ G. Piacente, I.V. Schweigert, J.J. Betouras, and F.M. Peeters, *Phys. Rev. B* **69**, 045324 (2004).
- ³⁸ I. Giaever, *Phys. Rev. Lett.* **15**, 825 (1965).
- ³⁹ J.R. Clem, *Phys. Rev. B* **9**, 898 (1974).
- ⁴⁰ J. Baker and A.G. Rojo, *J. Phys.: Condens. Matter* **13**, 5313 (2001).
- ⁴¹ C. Reichhardt, C. Bainsfather, and C.J. Olson Reichhardt, *Phys. Rev. E* **83**, 061404 (2011).
- ⁴² C. Bainsfather, C.J. Olson Reichhardt, and C. Reichhardt, *EPL* **94**, 18001 (2011).
- ⁴³ M.B. Hastings, C.J. Olson Reichhardt, and C. Reichhardt, *Phys. Rev. Lett.* **90**, 098302 (2003).
- ⁴⁴ C. Reichhardt and C.J. Olson, *Phys. Rev. Lett.* **89**, 078301 (2002); A. Pertsinidis and X.S. Ling, *Phys. Rev. Lett.* **100**, 028303 (2008).
- ⁴⁵ D.S. Fisher, *Phys. Rev. B* **31**, 1396 (1985).
- ⁴⁶ G. Grüner, *Rev. Mod. Phys.* **60**, 1129 (1988); C. Reichhardt, G.T. Zimányi, and N. Grønbech-Jensen, *Phys. Rev. B* **64**, 014501 (2001).
- ⁴⁷ A.C. Marley, M.J. Higgins, and S. Bhattacharya, *Phys. Rev. Lett.* **74**, 3029 (1995); C.J. Olson, C. Reichhardt, and F. Nori, *Phys. Rev. Lett.* **81**, 3757 (1998).